

ASSESSMENT OF MECHANICAL SHEAR RESPONSE USING DIGITAL IMAGE CORRELATION

AFERIÇÃO DO COMPORTAMENTO MECÂNICO EM CORTE UTILIZANDO CORRELAÇÃO DIGITAL DE IMAGEM

C. Leitão*, M. I. Costa **, D. M. Rodrigues***

*Investigador. CEMUC, Coimbra - Portugal.

**Investigadora. CEMUC, Coimbra - Portugal.

***Professora Auxiliar. CEMUC, Coimbra - Portugal.

RESUMO

No presente trabalho é descrita uma ferramenta especialmente desenvolvida para a realização de ensaios de corte simples, assim como os procedimentos utilizados durante o teste, para registo das deformações utilizando Digital Image Correlation (DIC). Os procedimentos desenvolvidos foram validados realizando ensaios em duas ligas de alumínio, vastamente utilizadas em construção soldada, a liga tratável termicamente AA6082-T6 e a liga não tratável termicamente AA5083-H111, que apresentam diferentes mecanismos de aumento de resistência, o que leva a que estas apresentem comportamentos mecânicos marcadamente diferentes a níveis consideráveis de deformação. Neste trabalho, foi ainda realizada uma análise microestrutural com o intuito de avaliar a precisão do uso desta técnica (DIC) no registo de gradientes de deformação na zona deformada dos provetes de corte. Foi assim possível constatar que a utilização de DIC permite aferir com exactidão o comportamento ao corte das duas ligas estudadas, assim como, registar a mais-valia que representa o uso de ensaios de corte na caracterização do comportamento mecânico de materiais, nomeadamente até grandes valores de deformação plástica, maiores do que aqueles registados durante os convencionais ensaios de tracção uniaxial.

ABSTRACT

In this work, a special tool, developed for running shear tests using a universal tensile testing machine is described, as well as the procedures used for strain data acquisition via Digital Image Correlation (DIC). Testing procedures were developed and verified by testing two aluminium alloys widely used in welding construction, the heat-treatable AA6082-T6 and the non-heat-treatable AA5083-H111 aluminium alloys, which are characterized by markedly different strengthening mechanisms, having completely different mechanical behaviour under large plastic deformations. Microstructural analyses were accomplished in order to evaluate the accuracy of strain data acquisition by DIC in capturing the strain gradients along the gage section of the shear samples. A good accuracy of results obtained using DIC to evaluate the shear response for both alloys, as well as the benefits of the shear test in assessing materials constitutive behaviour until very large values of plastic deformation, higher than those registered during conventional tensile testes was depicted.

1. INTRODUCTION

Nowadays, the continuous development of new materials, in addition to the continuous effort in improving and/or developing innovative industrial products,

makes mandatory the development of extensive and accurate techniques for assessing chemical and physical properties, as well as for characterizing the mechanical behaviour of the materials under complex loading conditions. As it is well known,

several tests regarding the characterization of metallic and non-metallic materials have already been developed and standardized. The most common between them, is the uniaxial tensile test, which is widely used for the assessment of mechanical properties at both the research and industrial levels. However, despite being a test of simple execution and having easy reproducibility of results, the tensile test doesn't supply enough information when the objective is to characterize the plastic behaviour of the materials under complex and/or severe plastic deformation conditions. In order to overcome this difficulty, the shear test appeared as an alternative approach for assessing mechanical properties under this type of solicitations. In fact, due to the delay in strain localization at maximum load, when compared to the uniaxial tensile test, the shear test allows the study of the mechanical behaviour under large deformations (Atkins, 1996) and to easily perform tests under reverse loading conditions (Bouvier, 2005) as well. Although no standards regulating shear testing procedures have already been developed, this mechanical test has already been used by several researchers for characterizing metallic materials, which developed distinct testing mechanisms (Bao, 2004; Reyes, 2009).

In this paper, a testing tool and testing samples specially conceived for testing thick material plates in simple shear, using a universal tensile testing machine, are presented. The accuracy of the developed testing procedure was evaluated by testing AA5083-H111 and AA6082-T6 aluminium alloys, which, as noticed in previous works from current authors (Leitão, 2012a), present markedly different plastic behaviours in tension. During the test, strain data acquisition was performed by using Digital Image Correlation (DIC), which also required developing and checking appropriate procedures for strain data analysis (Leitão, 2012b). Finally, in order to access the accuracy of the developed testing and strain data analysis techniques, the mechanical response registered in shear, for the AA5083 and

AA6082 alloys, is compared to that registered in uniaxial tension, by plotting equivalent stress-strain curves. Microstructural analysis was also accomplished in order to evaluate the accuracy of strain data acquisition by DIC in capturing the heterogeneous strain distribution across the gage section of the shear samples.

2. EXPERIMENTAL PROCEDURE

Two base materials, a non-heat-treatable (AA5183-H111) and a heat-treatable aluminium (AA6082-T6) alloy, widely used in transportation industries, were characterized in this study. The plastic behaviour of the base materials, supplied in 4 and 3 mm thick plates, respectively, was analysed by performing simple shear and tensile tests, using a 100kN universal testing machine (Instron 4206) in quasi-static conditions (5 mm/min). In order to characterize the anisotropy of both materials, the monotonic tensile tests were performed at 0, 45° and 90° to the rolling direction (RD). In both the tensile and shear tests, local strain fields were acquired by DIC using the Aramis 3D 5M optical system (GOM GmbH). Before testing, the specimens were prepared by applying a random black speckle pattern, over the previously mat white painted surface, in order to enable strain data acquisition by DIC. After testing, the gage sections of the shear samples were analysed, following standard metallographic practice, enabling to identify different deformation patterns. Metallographic analysis was performed using an optical microscope ZEISS HD 100.

3. DESCRIPTION OF SHEAR TESTING TOOL AND SHEAR SAMPLE GEOMETRY

In this work, a special tool enabling to perform simple shear tests was developed. The shear device, shown in Fig. 1a, works directly connected to a tensile testing machine, which promotes the parallel translation between the fixed and moving

parts of the tool, which are identified in the figure. The shear samples, whose geometry is shown in Fig. 1b, are placed in the tool with the aid of cylindrical guides (a in Fig. 1a) and fixed using grips (b in Fig. 1a). Tool design was conceived in order to avoid any rotation of the moving part of the tool, enabling the planar deformation of the sample during the test. In this way, as can be observed in Fig. 1c, where a scheme representing Section A in Fig. 1b is shown, the vertical translation of the moving part of the tool promotes the deformation in simple shear of the central section of the sample, with lower cross-section, labelled as shear zone in Fig. 1b. The samples' geometry was selected in order to avoid undesirable phenomena, such as buckling, stress concentration and abnormal strain distribution at the shear zone free-ends, which were reported by G'Sell, 1984, Bouvier, 2006a and Bouvier, 2006b in shear testing of very thin plates.

Due to the high relevance of the size of the homogeneous strain area, on shear testing results, several authors have already studied the influence of specimen dimensions on strain distribution. Bouvier et al. (2006b) stated that the size of the heterogeneous deformation area increases by decreasing the length (l_0) to width (h) ratio of the shear zone. In Fig. 1b, where the dimensions of the different shear samples features are shown, it is possible to depict that the maximum shear area width is 3 mm

(h) and the minimum shear length (l_0) is 20 mm. Actually, the circular geometry at the free-end of the shear zone, promotes a smooth variation of the h value and the maximization of the geometry factor (l_0/h), at the centre of the sample, which optimizes the homogeneous strain area size.

Due to its potential effect on load testing results, the friction load between the fixed and moving parts of the shear testing tool was measured. In Fig. 2 is compared the load versus time evolution for tests performed with and without sample. Observing the figure, it is possible to conclude that the load values for the test performed without sample are much lower than that registered in testing a sample, which allows concluding that the influence of the friction between the fixed and moving parts of the shear tool, on testing load results, is negligible.

In Fig. 3 is shown an image of the sample gage section before testing (Fig. 3a) and after plastic deformation, at maximum load (Fig. 3b). In Fig. 3b is also shown the corresponding vertical displacement map, acquired by DIC. Analysing this map, it is possible to conclude that the region marked as 1, corresponding to the part of the sample clamped to the fixed part of the shear tool, displays a uniform vertical displacement of 1.32 mm, indicating that the sample slipped slightly during testing. However, as stated by Bouvier et al. (2006b), the use of a noncontact optical

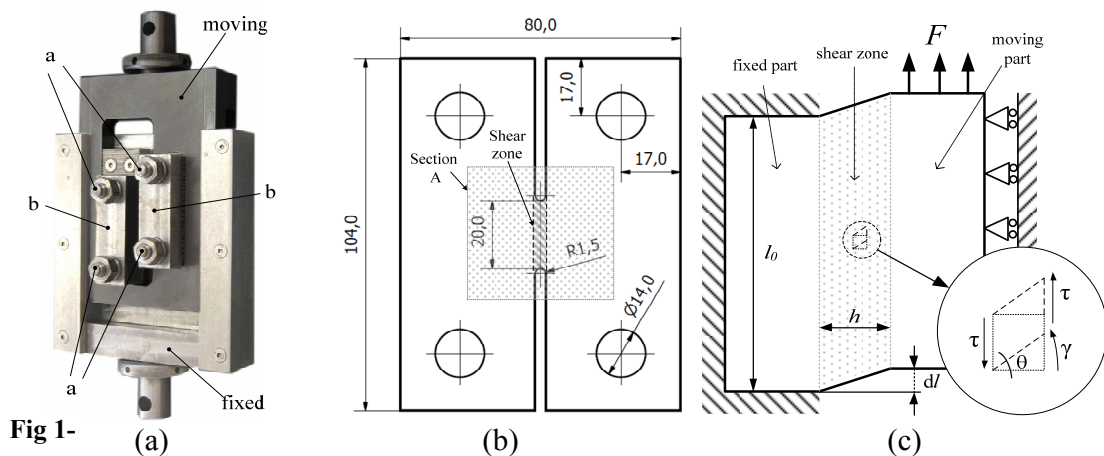


Fig. 1 Shear test tool (a), shear test sample geometry (b) and scheme of the shear zone behaviour under simple shear solicitation (c).

technique, such as DIC, for strain data acquisition, enables to eliminate the influence of any sample slipping during the test on strain measurement.

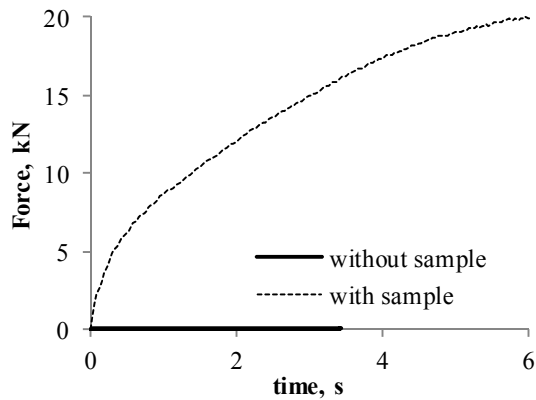


Fig.2 - Load (N) versus time (s) evolution in tests performed with and without sample.

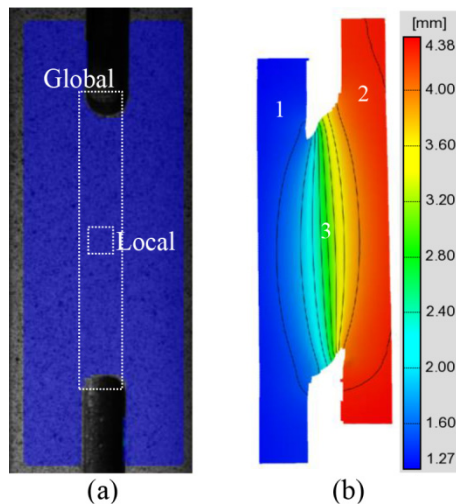


Fig.3 - Gage section before testing (a) and vertical displacement map at maximum load (b).

4. STRAIN DATA ANALYSIS

In Fig. 4a and Fig. 4b are shown ϵ_{xy} strain maps, calculated using ARAMIS software, at half of the maximum load ($F_{max}/2$) and at maximum load (F_{max}), for AA 5083 and AA 6082 samples, respectively. As it is possible to see in the figure, after yielding, an area of heterogeneous plastic deformation is formed along the shear zone, symmetric relative to the loading direction and to the sample middle-plane. The gradient in strain distribution becomes sharper at maximum load, when strain localization occurs at the free-ends of the shear zone. G'Sell et al.(1983) reported that

this strain concentration results, on one hand, from the constrain effect of the grips, reacting against the rotational moment imposed by the couple of shearing forces and, on the other hand, from the departure from ideal simple shear conditions, at the shear zone free-end, where stresses normal and parallel to the sample surfaces develop. The localized transverse tensile stresses, at the shear zone free-ends, promote the strain localization at maximum load.

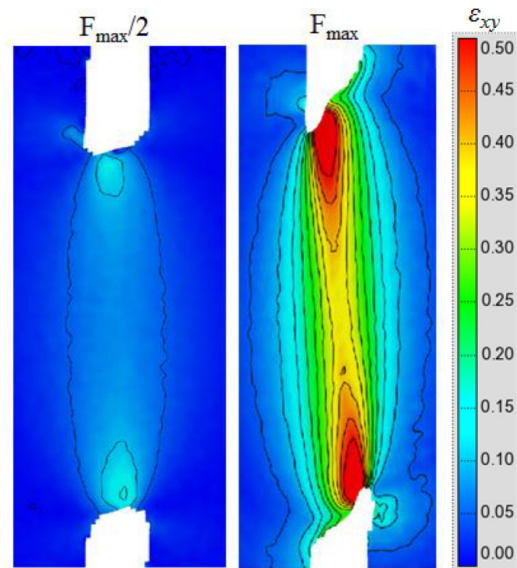


Fig. 4a - Strain maps (ϵ_{xy}) at half of maximum load ($F_{max}/2$) and at maximum load (F_{max}) for the AA5083 alloy.

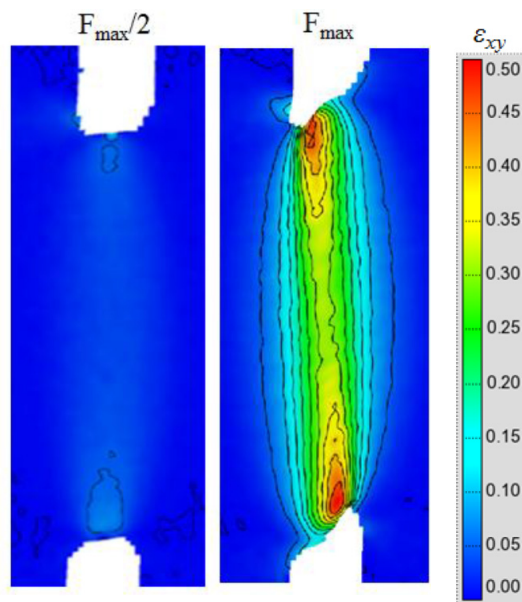


Fig. 4b - Strain maps (ϵ_{xy}) at half of maximum load ($F_{max}/2$) and at maximum load (F_{max}) for the AA6082 alloys.

In order to evaluate the accuracy of the strain data acquisition by DIC in capturing the strain gradients across the gage section, metallographic analyses were performed in order to identify different deformation patterns across the shear zone. The microstructural evolution near the fracture zone of AA5083 and AA6082 shear samples is shown in Fig. 5 and Fig. 6, respectively. In these pictures it is possible to see the evolution in grain shape and orientation, from the non-deformed part of the sample, to the fracture surface. The evolution of the angle between the initial grain orientation and the normal to the loading direction (θ) was measured, being marked in both micrographs. In both figures are also shown shear angle maps (γ), obtained by DIC, after maximum load, for the same samples. Since the shear angle (θ) and the shear strain (γ) may be related through the expression

$$\gamma = \tan \theta \cong \theta, \quad (1)$$

the results from the metallographic analysis were compared with DIC measurements, as is shown in the graphs of Fig. 7a and Fig. 7b, for the AA5083 and AA6082 alloys, respectively. In each of these graphs, the evolution of θ and γ with the distance to the fracture surface of the samples is plotted, considering the sample sections marked by black lines in each strain map of the Fig. 5 and Fig. 6. From the graphs it is possible to depict that both type of results are in very good agreement.

For each sample tested, the strain path evolution with plastic deformation, inside the shear zone, was also analysed in order to verify if the simple shear loading conditions prevail until maximum load, in spite of the non-uniform strain distribution depicted in previous figures. The major (ϵ_1) versus minor strain (ϵ_2) evolution, which is representative of the strain path evolution during loading, is shown in Fig. 8a and Fig. 8b, for the AA5083

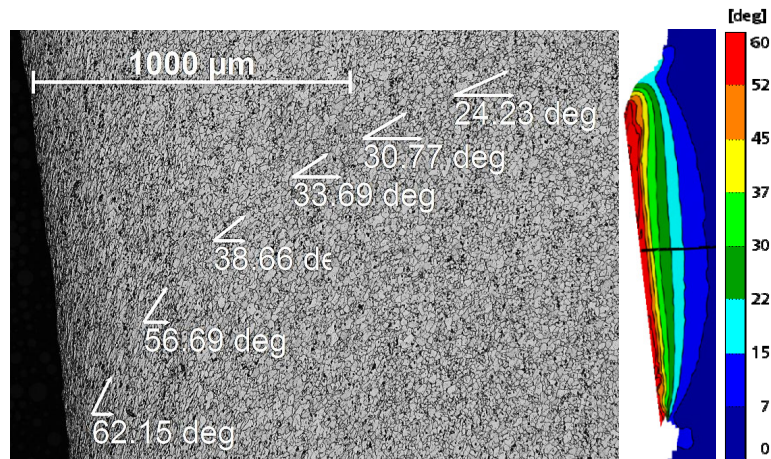


Fig.5 – Evolution of grain orientation (θ), from micrographic analysis, and shear strain angle (γ), assessed by DIC, for the AA5083-H111 alloy.

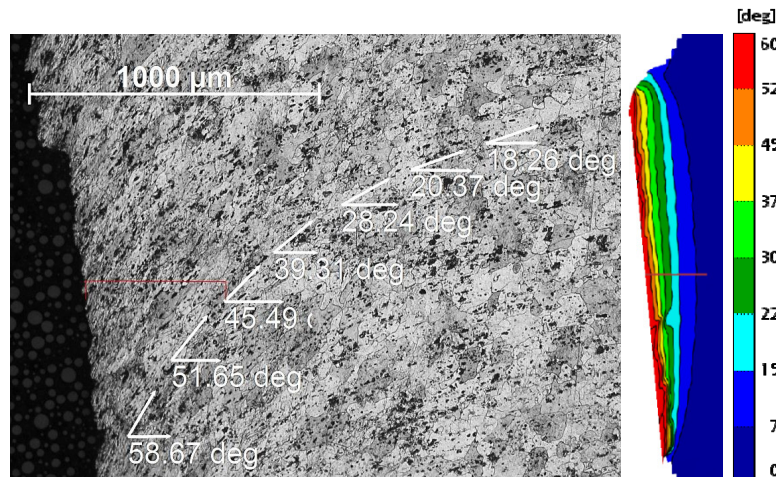


Fig.6 – Evolution of grain orientation (θ), from micrographic analysis, and shear strain angle (γ), assessed by DIC, for the AA6082-T6 alloy.

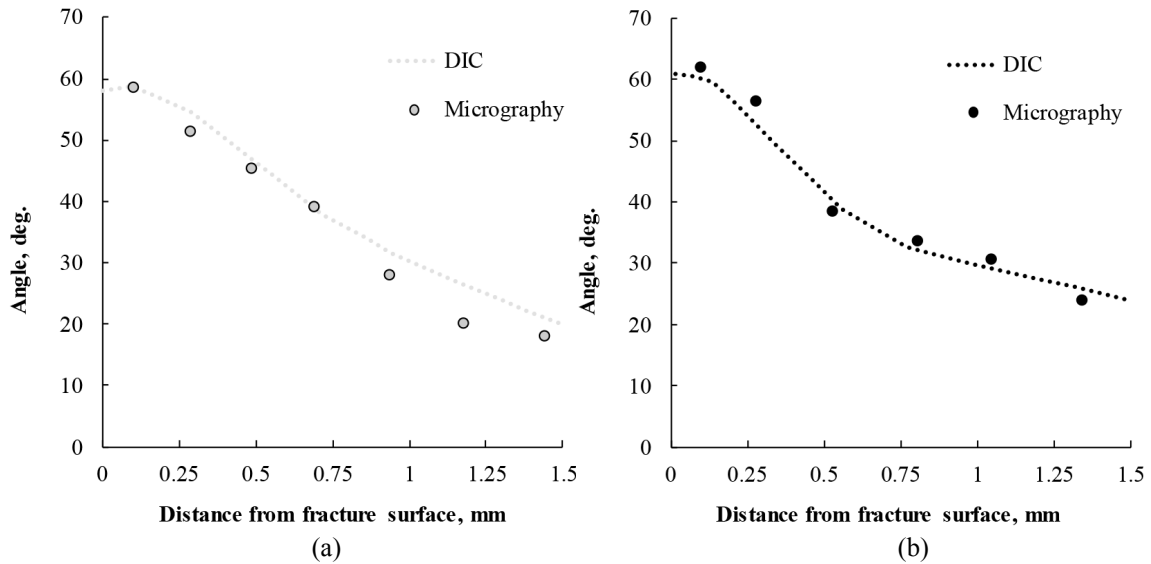


Fig 7 - Evolution of grain orientation (θ), from micrographic analysis, and shear strain angle (γ), assessed by DIC, for the AA5083-H111 (a) and AA6082-T6 (b) alloys

and AA6082 alloys, respectively. The results plotted in the graphs, correspond to average strain values calculated using Aramis software. Two evaluation areas were considered for calculating the average strains ϵ_1 and ϵ_2 , which are identified as Local and Global in Fig. 3a. Using the Global evaluation area, the full range of strain values registered in the shear zone is considered for computing the average strains. Using the Local evaluation area, only the strain values at the centre of the sample, where the strain fields are homogeneous, are considered in computing the average strains.

Analysing Fig. 8 results, for both alloys, it is possible to conclude that pure-shear conditions ($\epsilon_2 = -\epsilon_1$) prevail until maximum load, independently of the strain evaluation area considered. Actually, no strain path change is observed, even considering the global evaluation area, which allows concluding that the free-end influence on strain distribution, inside the shear zone, has no significant influence on global strain path evolution.

5. STRESS-STRAIN ANALYSIS

Using the strain data acquired by DIC, shear stress-strain curves (τ, γ) were computed, considering the Local and Global strain evaluation areas indicated in Fig. 4a for calculating the average strain (γ)

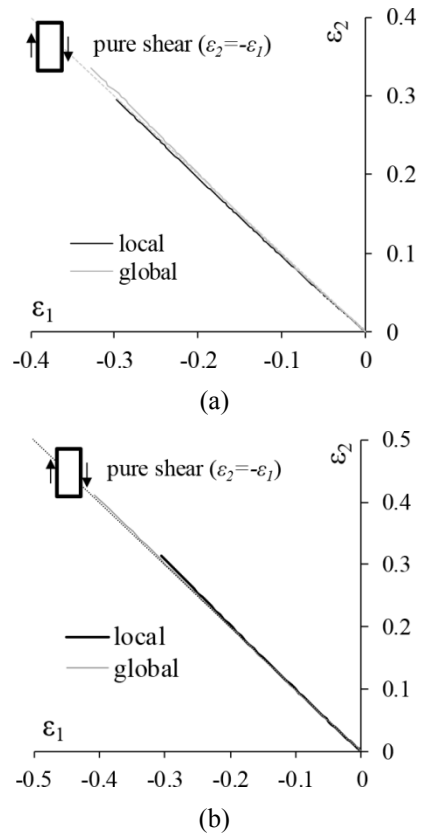


Fig. 8 - Strain path evolution for the AA5083 (a) and AA6082 (b) samples during shear testing.

in the shear zone. Assuming iso-stress conditions during shear testing, the shear stress (τ) was obtained by dividing the testing load (F) by the shear zone cross-section area (A), according to the equation

$$\tau = \frac{F}{A} = \frac{F}{l_0 \times t} \quad (2)$$

where, l_0 and t are the length and thickness of the shear zone, respectively. In the same way, the shear strain (γ) was obtained considering the relation

$$\gamma = 2\varepsilon_{xy}. \quad (3)$$

The Local and Global average shear stress-strain curves (τ - γ) are plotted in Fig. 9, where it is possible to depict an excellent concordance between both types of results. This shows that the non-uniform shear strain distribution, depicted in previous analysis, does not influence significantly the shape of curves. The only difference between Local and Global results is that the strain values, corresponding to the global strain average, are significantly higher than the local average strain values, corresponding to the local area with homogeneous strain distribution, at the centre of the sample.

Analysing the shear stress-strain curves, it is possible to conclude that the AA6082 alloy, after moderate values of plastic deformation, presents an almost steady-state flow stress, which is in accordance to that reported by Rauch et al., 2002, for other aluminium alloys of the 6xxx series. On the other hand, for the AA5083 alloy, which displays lower yield strength than the AA6082 alloy, the flow stress keeps increasing with loading. Actually, the AA5083 alloy attains strength values higher than that of the AA6082 alloy, after some

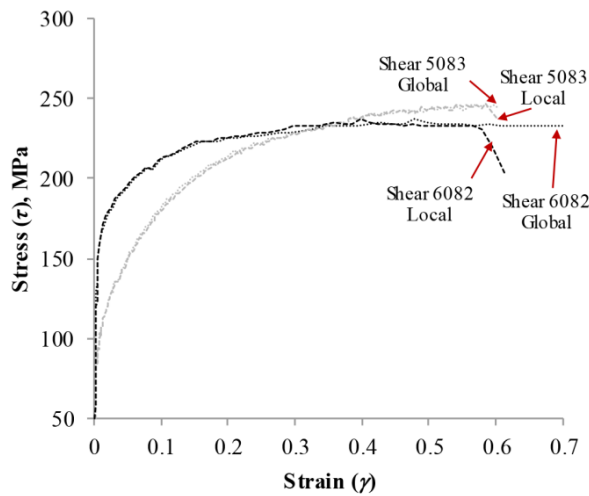


Fig. 9 - Shear stress-strain curves: Local and global.

plastic deformation. The differences in strain-hardening behaviour determine the shape and size of the plastic deformation area, at the centre of the sample, which as shown in Fig. 4, is narrower for the AA6082 alloy, than for the AA5083 alloy. Actually, the AA5083 displays a wider plastic deformation zone, with a belly form, for the same strain range of the AA6082, due to its stronger hardening sensitivity.

Finally, in Fig. 10 are compared the equivalent stress-strain curves corresponding to uniaxial tensile tests and shear tests, for both alloys. The equivalent stress-strain curves were obtained using the Hill'48 plasticity criteria (Hill, 1948)

$$\begin{aligned} & F(\sigma_{yy} - \sigma_{zz})^2 + G(\sigma_{zz} - \sigma_{xx})^2 + \\ & + H(\sigma_{xx} - \sigma_{yy})^2 + 2L\tau_{yz}^2 + \\ & + 2M\tau_{zx}^2 + 2N\tau_{xy}^2 = 1 \end{aligned} \quad (4)$$

where σ_{xx} , σ_{yy} , σ_{zz} , τ_{xy} , τ_{xz} and τ_{yz} , are the components of the Cauchy stress tensor, defined in the orthotropic frame, and F , G , H , L , M and N are the Hill coefficients of anisotropy. The Hill48 coefficients were calculated according to the equations

$$F = \frac{r_0}{r_{90}(1+r_0)} \quad (5)$$

$$G = \frac{1}{1+r_0} \quad (6)$$

$$H = \frac{r_0}{1+r_0} \quad (7)$$

$$N = (r_0 + r_{90}) \frac{(2r_{45} + 1)}{2r_{90}(1+r_0)} \quad (8)$$

where r_0 , r_{45} and r_{90} are the anisotropy coefficients determined by performing tensile tests at 0, 45 and 90° from the rolling direction. In Table 1 are shown the anisotropy coefficients and the Hill48 coefficients determined for both alloys.

Observing Fig. 10, it is possible to conclude that, until moderate values of plastic deformation ($\varepsilon \approx 0.1$), the tensile and shear equivalent stress-strain curves are in excellent concordance, for both alloys.

Table 1 – Anisotropy coefficients

	r_0	r_{45}	r_{90}	F	G	H	N
AA5083	0.607	0.521	0.608	0.621	0.622	0.378	1.269
AA6082	0.681	0.576	0.699	0.580	0.595	0.405	1.264

However, for higher levels of plastic deformation, the tensile curves become higher than the shear curves, which points for the limitations of the Hill48 criteria in describing aluminium alloys behaviour, as already stated by other authors (Wang and Lee, 2006).

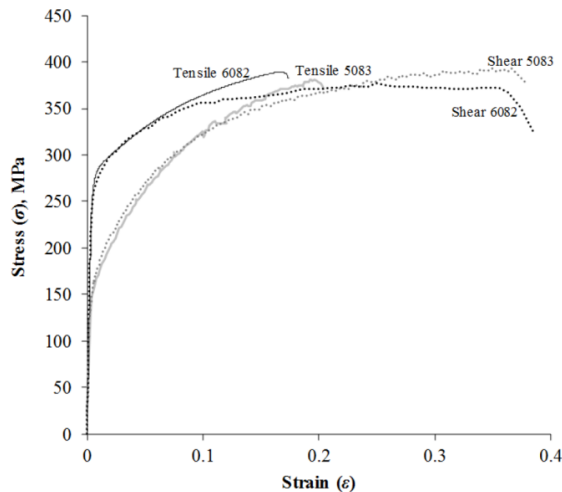


Fig. 10 – Tensile and Shear equivalent stress-strain curves.

6. CONCLUSIONS

From current study, it was possible to depict the good accuracy of results obtained using DIC to evaluate the shear response for the AA5083 and AA6082 alloys, as well as the benefits of the shear test in assessing materials constitutive behaviour until very large values of plastic deformation. The shear data was validated by comparing shear equivalent stress-strain curves, calculated using the Hill48 criterion, with the ones obtained in uniaxial tension. For both alloys, the concordance between shear and tensile curves, for moderate values of plastic deformation, was evident. The shear testing procedure developed in current work is now prone to be used in assessing the plastic properties of thick plates, with special relevance for the local characterization of the plastic properties of welds, for which the limited width of the sampling area makes the mechanical characterization in tension very hard.

ACKNOWLEDGEMENTS

The authors indebted to the Portuguese Foundation for the Science and Technology (FCT) and FEDER for the financial support.

REFERENCES

- Atkins AG. Fracture in forming. *Journal of Materials Processing Technology*. 1996, 56, p. 609-618.
- Bao Y, Ghosh AK. On fracture locus in equivalent strain and stress triaxiality space. *International Journal of Mechanical Sciences*. 2004, 46, p. 81-98.
- Bouvier S, Alves JL, Oliveira MC, Menezes LF. Modelling of anisotropic work-hardening behaviour of metallic materials subjected to strain-path changes. *Computational Materials Science*. 2005, 32 (3–4), p. 301-315.
- Bouvier S, Gardey B, Haddadi H, Teodosiu C. Characterization of the strain-induced plastic anisotropy of rolled sheets by using sequences of simple shear and uniaxial tensile tests. *Journal of Materials Processing Technology*. 2006, 174, p. 115-126.
- Bouvier S, Haddadi H, Levée P, Teodosiu C. Simple shear tests: Experimental techniques and characterization of the plastic anisotropy of rolled sheets at large strains. *Journal of Materials Processing Technology*. 2006, 172, p. 96-103.
- G'Sell C, Boni S, Shrivastava S. Application of the plane simple shear test for determination of the plastic behaviour of solid polymers at large strains. *Journal of Materials Science*. 1983, 18, p. 903-918.
- Hill R. A theory of the yielding and plastic flow of anisotropic metals. *Proceedings of the Royal Society A*, 1948, 193, p. 281-297.
- Leitão C, Louro R, Rodrigues DM. Analysis of high temperature plastic behaviour and its relation with weldability in friction stir welding for aluminium alloys AA5083-H111 and AA6082-T6. *Materials and Design*. 2012, 37, p. 402-409.

- Leitão C, Galvão I, Leal RM, Rodrigues DM. Determination of local constitutive properties of aluminium friction stir welds using digital image correlation. *Materials and Design*. 2012, 33, p. 69–74.
- Rauch EF, Gracio JJ, Barlat F, Lopes AB, Duarte Ferreira J. Hardening behaviour and structural evolution upon strain reversal of aluminium alloys. *Scripta Materialia*. 2002, 46, p. 881-886.
- Reyes A, Eriksson M, Lademo O-G, Hopperstad OS, Langseth M. Assessment of yield and fracture criteria using shear and bending tests. *Materials and Design*. 2009, 30, p. 596-608.
- Wang L, Lee TC. The effect of yield criteria on the forming limit curve prediction and deep drawing process simulation. *International Journal of Machine Tools and Manufacture*. 2006, 46, p. 988-995.

